Filtering and Modulation from the Infrared to the Terahertz using Phase-Change Extraordinary Optical Transmission Metasurfaces

Euan Humphreys[1], Jacopo Bertolotti[1], Carlota Ruiz de Galarreta[1,2], Noemi Casquero[2], Jan Siegel[2] and C. David Wright[1]

[1]Centre for Metamaterials Research and Innovation, Exeter University of Exeter, Exeter, UK
[2]Laser Processing Group, Instituto de Óptica, IO-CSIC, 28006 Madrid, Spain.
E-mail: david.wright@exeter.ac.uk

Keywords: extraordinary optical transmission, tunable filter, phase-change metasurface, multispectral sensing

Periodic arrays of sub-wavelength-scale holes in plasmonic metal films are known to provide resonant transmission peaks via the extraordinary optical transmission (EOT) effect. Active control of the spectral position of such transmission peaks can be obtained by adding a layer of phase-change material (PCM) to the EOT device. Switching the PCM layer between its amorphous and crystalline states can shift the spectral position of the resonance, enabling potential applications in the fields of active filtering and sensing (e.g. multispectral sensing), and for signal modulation. Here we report the design, fabrication and characterisation of active EOT devices targeted at various important regions of the optical spectrum.

1. Introduction

In the extraordinary optical transmission (EOT) effect the transmission of light through an array of sub-wavelength holes in an otherwise opaque metallic film, is greatly enhanced, primarily due to the role played surface plasmons[1]. The wavelength and amplitude of the EOT transmission peak are dependent on the array geometry (primarily hole spacing/array pitch) and the optical properties of materials "surrounding" the EOT array. Usually, such surrounding materials consist of the substrate material on one side of the metallic film, and air on the other. If, however, a phase-change material such as one of the well-known chalcogenide PCM alloys is deposited onto the EOT array, the wavelength of the transmission peak can be controlled[2,3] by switching the PCM layer between its

This article has been accepted for publication and undergone full peer review but has not been through the copyediting, typesetting, pagination and proofreading process, which may lead to differences between this version and the Version of Record. Please cite this article as doi: 10.1002/pssr.202200474.

amorphous and crystalline states (or to some intermediate fractionally crystallised state), since the refractive index of PCMs is very different in its different solid states. Since PCMs can in principle be switched on the nanosecond type scale, this opens up the possibility for EOT-based devices incorporating PCM layers to provide fast, active, tunable bandpass filtering, with a tuning range influenced by the change (between amorphous and crystal states) in the real part (n) of the refractive index. Such fast, dynamically tunable bandpass filters in turn would be extremely useful for multispectral sensing and imaging, which finds widespread application in areas ranging from agricultural and environmental monitoring, to missile detection, chemical sensing and more[4-7]. Conventional multispectral systems typically use multiple sets of narrowband sensors (one per waveband), or a broadband sensor with a set of mechanically switchable narrowband filters, both approaches leading to, in general, bulky, slow and relatively costly implementations. Such multi-filter systems could potentially be replaced with a single (or relatively small number) of EOT-PCM based active filters, leading to considerably more compact and faster multispectral systems, so long as sufficiently narrow bandpass responses, and overall bandwidth coverage, can be obtained (by EOT-PCM based devices) for the particular application in question. In this paper, therefore, we explore the design, fabrication and characterisation of tunable EOT-PCM based filters, primarily for operation in the mid-infrared (MWIR). We compare two approaches for the fabrication of the EOT arrays themselves, the commonly-used, high-precision but slow e-beam lithography route, and a much faster and readily scalable (to large device sizes) method employing ultrafast direct laser writing. We also extend our designs out to the THz waveband, where, at least for the PCM compositions used here, relatively large values of the imaginary part (k) of the refractive index in the crystalline state lead to an on/off EOT type response (rather than bandpass filtering), which may find application for THz modulation. Finally, since EOT films are invariably fabricated using the archetypal plasmonic metals Au and Ag, and since Au and Ag diffuse readily into PCMs resulting in a change in PCM layer properties and an associated degradation of optical performance[8,9], we report the effects of such diffusion on EOT-PCM devices.

2. Design and Fabrication of EOT Arrays

The passage of light through a single sub-wavelength hole classically results in very poor transmission efficiency, on the order of $\sim(r/\lambda)^4$, where r is the hole radius and λ the wavelength[10]. The transmission can be improved by many orders of magnitude utilising ordered arrays of sub-wavelength holes in a thin plasmonic metal film (e.g. Au and Ag[11,12]). This results in the EOT effect, where the primary mechanism is the coupling of the incident light to surface plasmons (SPs) on the top (incident) surface, which in turn excites SPs on the bottom surface, re-illuminating the

holes. A finite-element simulation (using COMSOL Multiphysics™) of a typical EOT transmission spectrum in the MWIR is shown in **Figure 1**, along with plots of the electrical field distribution at the (bottom) film surface. The EOT spectrum has a characteristic asymmetric Fano-type resonance (arising from a periodic perturbation, here a square lattice), along with evidence of Wood-Rayleigh anomalies at wavelengths just below the resonant wavelength [1,13]. The E-field plots show clearly the generation of high fields at the hole edges at the peak transmission wavelength.

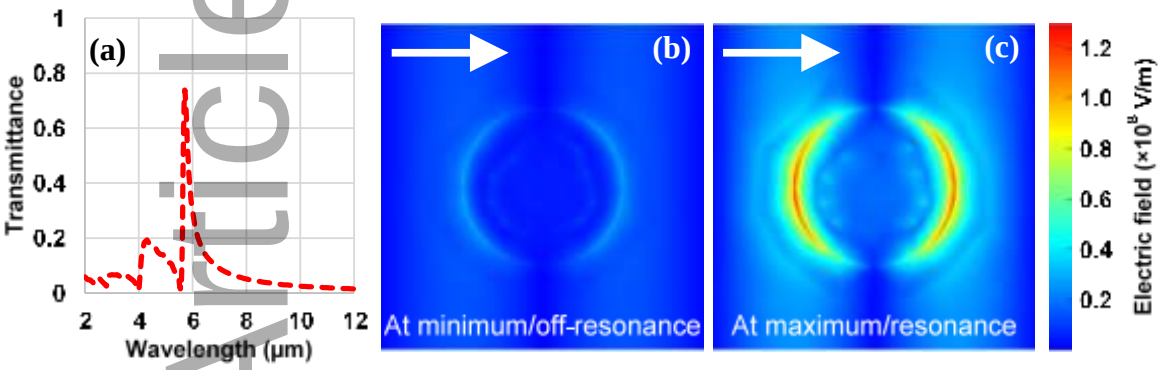

Figure 1. (a) Simulated transmission spectrum of a 4 μm-pitch EOT square array with 2 μm circular holes in 40 nm Au film on a CaF_2 substrate), and simulated E-field distribution on (b) the bottom of the film surface (i.e. non-incident surface) away from the peak transmission wavelength and (c) at the peak transmission wavelength.

The position of the peak of transmission is determined primarily by the array pitch p and refractive index n of the material at the film interfaces[3], and red-shifted with respect to the preceding minima defined by the Rayleigh wavelengths at the Au-CaF_2 interface ($\lambda_R \approx n_{CaF2}p$) and Au-air interfaces ($\lambda_R \approx p$). **Figure 2** shows simulated and measured (using Fourier Transform Infrared spectroscopy, or FTIR, techniques) EOT transmission spectra, demonstrating the effect of changing the array pitch with all materials and other dimensions (most importantly hole diameter relative to array pitch) kept constant. Designs can thus be optimized for peak transmission at specific wavelength; here we concentrate on the MWIR (and later THz) regime.

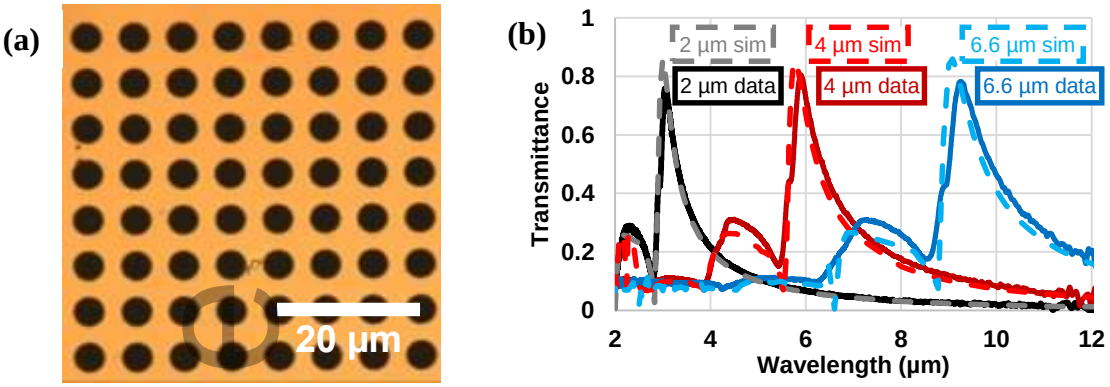

Figure 2. (a) Optical microscope image of an EOT array in an Au film and (b) measured (using FTIR) transmission spectra of EOT arrays of varying pitches (2, 4 and 6.6 µm) in a 40 nm Au film on CaF_2 substrates (solid lines), along with finite-element simulated equivalents (dashed lines).

The standard approach to the fabrication of EOT arrays is e-beam or optical lithography (depending on the feature size). For the arrays shown in Figure 2 we used e-beam patterning on evaporated gold films, following a process as outlined in **Figure 3(a)**. Such a process provides fine, near-perfect control of dimensions; a disadvantage however is the large number of steps required, increasing both the fabrication cost and time necessary to complete the process. Scale-up to very large array sizes is also not straightforward using e-beam patterning techniques (at least not in reasonable times). We therefore developed a fabrication technique based on ultrafast laser processing for the rapid realisation of EOT metasurfaces[14]. This consists of patterning holes into gold films via direct laser-ablation, employing an ultrafast pulsed laser and a motorised stage, as briefly shown in **Figure 3(b)**. This approach is capable of controlling both the array period and the hole diameter, with areal patterning rates limited in practice only by the speed of the scanning stages.

In order to assess the potential of the laser ablation approach for future mass-production of EOT-based devices, EOT arrays having different geometries were fabricated using both the laser processing method and the more conventional e-beam lithography (and wet etching) technique, and their optical performances compared (using FTIR). Results are shown in **Figure 4**, in which it can be seen that there is a good correspondence in terms of spectral response across the two methods (very similar peak transmission wavelengths, similar Q factors). It is noticeable that the laser ablated EOT arrays generally have reduced absolute transmission values as compared to the e-beam patterned samples. This is likely due to stitching errors (i.e. hole position imperfections causing non-perfect square lattices) caused by stage positioning errors in the laser fabrication approach (refinements to eliminate such stitching errors are currently being carried out). A more detailed comparison of the

EOT transmission spectra for the two fabrication methods is given in **Table 1,** along with other key fabrication process parameters, in particular fabrication speed/time.

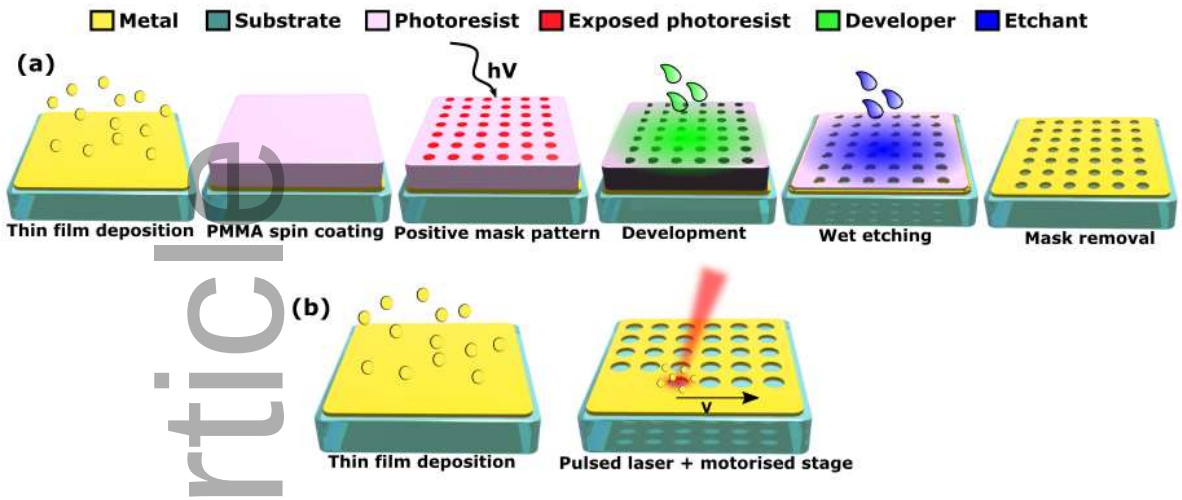

Figure 3. Fabrication of EOT arrays using **(a)** conventional e-beam lithography and **(b)** a single-step laser-ablation processes. (Reprinted (adapted) with permission from C R de Galarreta et al., ACS Appl. Mater. Interfaces 2022, 14, 2, 3446; Copyright American Chemical Society 2022)

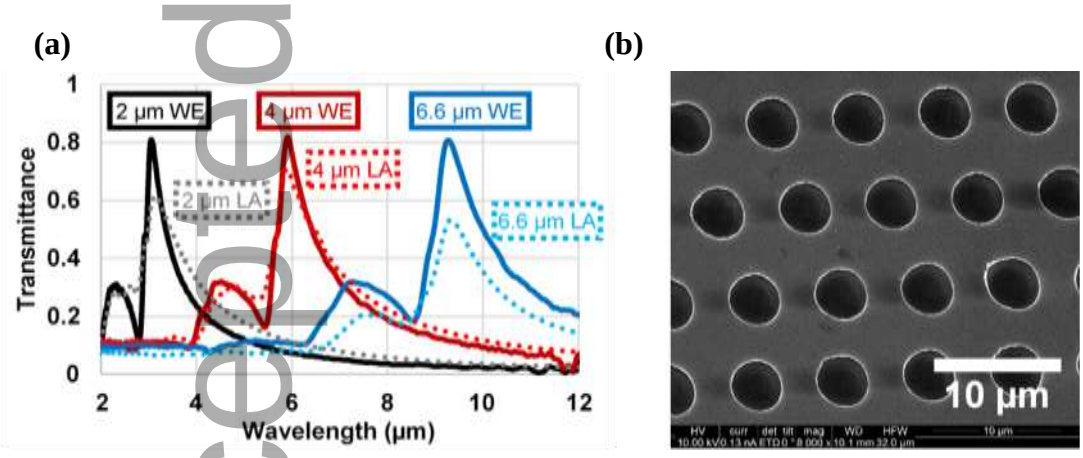

Figure 4. (a) Transmission spectra of (solid lines) e-beam/wet-etching fabricated EOT arrays (dotted lines) and the corresponding laser fabricated versions, and (b) SEM image of a typical laser fabricated EOT array, showing the nature of stitching errors.

Table 1. Comparison of EOT array fabrication methods

Period (μm)	Method	Max T	Q-factor	Time	Fabrication steps

2	**WE**	**0.81**	**4.99**	**Few hours**	**6**
	LA	0.61	2.43	19 minutes	2
4	**WE**	**0.82**	**5.66**	**Few hours**	**6**
	LA	0.71	4.09	10 minutes	2
6.6	**WE**	**0.81**	**6.08**	**Few hours**	**6**
	LA	0.53	5.39	3 minutes	2

3. Tunable EOT-PCM Filters for the MWIR Spectral Regime

To add tunability to the basic spectral response of an EOT array, a simple and practicable approach is to deposit a thin layer of PCM alloy directly on to the top of it, such that the PCM layer covers the metal film and fills the holes themselves, yielding a device configuration as shown in **Figure 5**. Key properties of the PCM that determine the resulting optical response are its refractive index *n* and extinction coefficient *k*; the former will affect the position of the transmission peak, while the latter introduces absorption/damping and would be expected to lead to a reduction in peak transmission amplitude along with a broadening of the peak itself. Since *n* and *k* can differ very considerably between the amorphous and crystalline states of a PCM, we expect to see shifts in the peak transmission wavelength, and changes in transmission amplitude (and Q factor) when the PCM layer is switched between these states. Preferably, for the tunable filter application, the change in *n* between states should be large, so leading to a significant shift in the peak transmission wavelength, while changes in *k* should be small, so that the transmission amplitude does not vary too significantly on switching (ideally k would be vanishingly small in both states).

The variations of *n* and *k* as a function of wavelength in the MWIR range for two commonly used GeSbTe PCM alloy compositions, $Ge_2Sb_2Te_5$, (GST-225) and $Ge_3Sb_2Te_6$ (GST-326) are shown in **Figure 6** (and taken from Michel et al.[15]). It can be seen that the difference in *n* values (between crystal and amorphous states) over the wavelength shown is slightly larger for GST-326 *cf.* GST-225, that the *k* value for both alloys is small in the amorphous state, and that the *k* value in the crystalline state is smaller (over most of the wavelength range shown) for GST-326. Thus, we would expect slightly larger shifts (on switching from amorphous to cystalline states) of the peak transmission wavelength for the GST-326 composition, along with less relative reduction in peak transmission amplitude.

(a) **(b)**

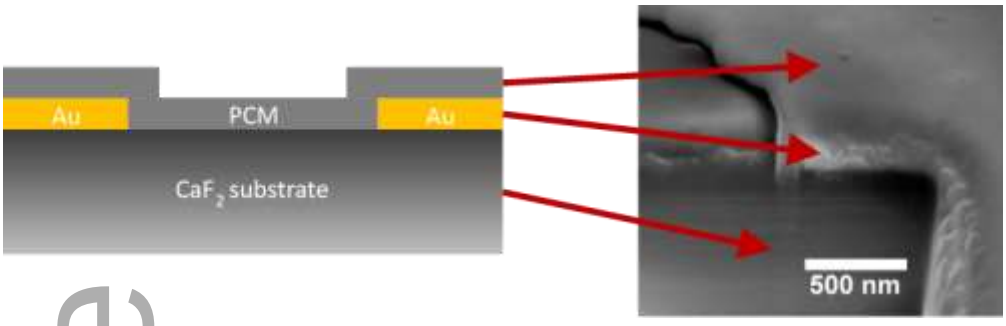

Figure 5. (a) Schematic cross-section of and EOT device with a thin PCM layer deposited on to it, covering the metal and filling the holes in the array, and (b) cross-sectional SEM image of an as-fabricated device, trench milled at the hole edge via focused ion beam milling.

EOT-PCM devices were fabricated (using e-beam lithography) on hole arrays in 40 nm thick Au films on CaF substrates and using both GST-225 and GST-326 compositions. The PCM layers were deposited using magnetron sputtering and had thicknesses between 70 nm and 100 nm. An 8 nm Si_3N_4 capping layer to prevent PCM degradation after exposure to air (especially while heating) was deposited on top of the PCM, and on some samples an interfacial barrier layer (also 8 nm of Si_3N_4) was deposited between the Au and PCM layers as part of study of diffusion effects (see **Section 4**). We found (via both simulation and experiment) that 8 nm thick Si_3N_4 layers had no significant effect on the optical properties (transmission spectra) of the devices. Device transmission spectra were measured using FTIR spectroscopy, with scans being normalised to the transmission of a blank CaF_2 substrate (~95% from 2-8 μm). After measuring in the amorphous state, samples were heated on a hotplate to crystallise the PCM layer (the GST-225 layer over a range of temperatures from 150^0C to 200^0C for a total of 7 minutes, the GST-326 sample at 300^0C for 5 minutes). Typical results are shown in Figure 6 for both compositions (along with simulations for the GST-225 case). For devices fabricated with GST-225, a red shift of the peak transmssion wavelength of 1.03 μm (or approximately 14.9%) was observed, while for GST-326 a slightly larger shift of 1.10 μm (or approximately 16.3%) occurred, the relative shifts in line with expectations. For GST-326, post-crystallisation the relative peak amplitude transmission is also slightly higher, and the Q-factors of the peaks are larger, as we would expect from its lower *k* value with respect to GST-225. Even lower *k* values in the crystalline phase could be obtained, so resulting in higher transmission values in the crystalline state, by using recently developed low-loss materials, such as Se-substituted GeSbTe compositions reported by Zhang et al.[16]. We also note that our MWIR EOT-PCM devices always show asymmetric transmission peaks (reflecting the inherent asymmetric nature of the EOT effect itself, and particularly evident in the relatively low-*k*

amorphous phase), that the transmission peaks are relatively broad (Q-factors in this wavelength range for our devices were typically in the range of 2.5 to 5) and that the crystalline peak transmission is always significantly lower than that in the amorphous phase. We do not observe the symmetric, narrow, high-Q type responses reported for both phases by Julian et al.[17].

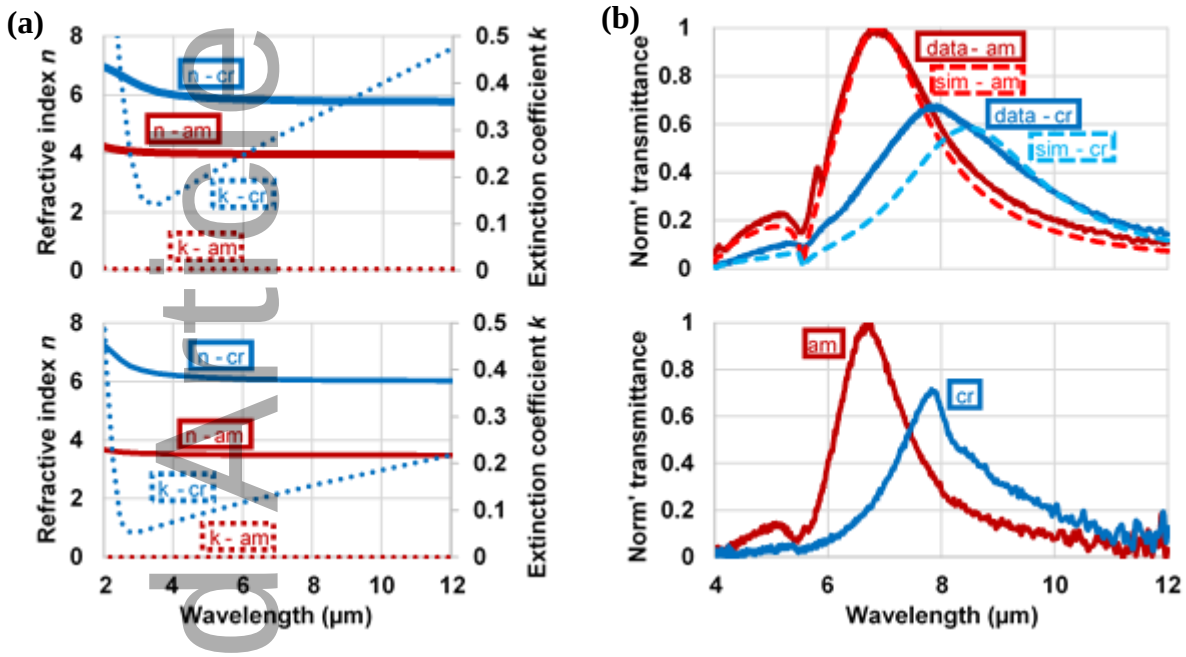

Figure 6. (a) Optical properties of GST PCMs (as reported by Michel et al.[15]), and (b) transmission spectra of tunable MWIR EOT-PCM filters fabricated in GST-225 (top) and GST-326 (bottom) with 4 μm EOT hole array periods. Note that the spectra are here normalised by the peak transmission in the amorphous case (the absolute value of transmission was 0.9 in the case of the GST-225 sample, which was 70 nm in thickness, and 0.57 for the GST-326 sample, which was 100 nm thick). Simulated spectra for the GST-225 case are also given, and show relatively good agreement with the experimentally obtained results.

4. EOT-PCM Devices in the THz Regime

As we have seen, the transmission characteristics of EOT-PCM devices depend on the optical properties (*n* and *k*) of the PCM layer itself. In particular we saw that in the crystalline state, where commonly used PCMs typically have non-negligible *k* values in the MWIR range, the peak transmission amplitude is reduced. In the THz range, *k* values for the PCM crystalline state can be much higher than those in the MWIR, as reported for archetypal PCM composition GST-225 by Makino et al.[18] (see **Figure 7**). Indeed, *k* is so high in the crystalline phase in the THz band that we can use EOT-PCM devices as a form of modulator, rather than as a tunable bandpass filter. We

show some examples of such modulators in **Figure 7**, here in simulation only, for the case of EOT hole arrays with a pitch of 175 µm (to create devices with peak modulation at around 1 THz, or ~300 µm) in 100 nm Au films on quartz substrates, and with a 100 nm GST-225 layer. The relative diameter *d* of the holes to the pitch *p* was varied and the absolute transmission and modulation depth (T_{am}/T_{cr}) over a range of frequencies from 0.6 to 1.4 THz calculated. The results are shown in Figure 7, where it can be seen that high modulation depths can be achieved (here >30) and that smaller holes lead to a higher Q-factor and modulation depth, whereas larger holes give greater absolute transmission. We note that in work carried out in parallel to our studies of THz EOT-PCM modulators, Cao et al.[19] recently reported the experimental realisation of such devices.

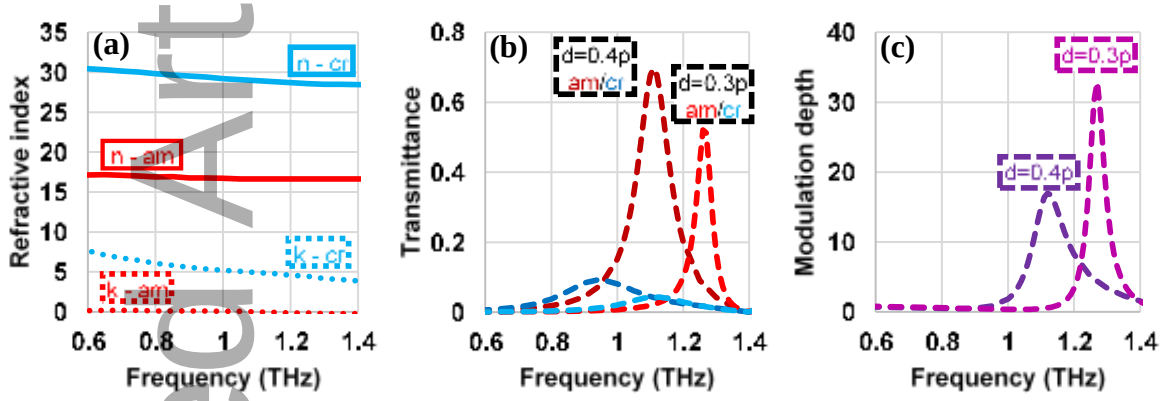

Figure 7. (a) Optical properties of GST-225 at THz wavelengths as reported by Makino et al.[18], and finite-element simulated transmittance (b) and modulation depth (c) of EOT-PCM THz modulators.

5. Metal/PCM Diffusion Issues

As briefly mentioned in §3 above, a potential problem when combining PCM films with typical plasmonic metals, such as Au, is that of interdiffusion. Indeed, Au tends to diffuse readily into PCMs, with the potential for the formation of gold tellurides[3]. This can lead to a significant degradation of optical properties and performance in device applications[3,9]. In the case of EOT-PCM devices, the effects of Au diffusion result in suppression of the transmission resonance and, eventually, rendering the device no longer "switchable". Such effects are evident in **Figure 8**, where the transmittance of a GST-225 EOT filter device (indeed the one previously shown in Figure 6) after prolonged heating is shown. This device had no barrier layer between the Au and PCM films, leading to extensive gold diffusion (as indicated by the microscope images also shown in Figure 8).

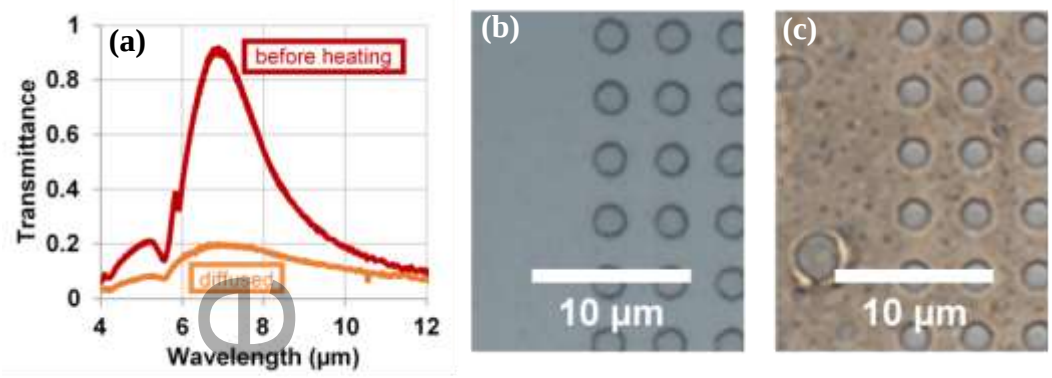

Figure 8. (a) Transmission spectrum of the GST-225 EOT device previously shown in Figure 6, before and after extended heating (below 300 °C), showing the deleterious effects of Au diffusion on device optical performance. Also shown are optical microscope images of similar devices (b) before and (c) after heating, where the effects of Au diffusion are clearly seen.

While the use of alternative materials more resistant to diffusion into PCMs is potentially viable for EOT-based devices (e.g. titanium nitride having been demonstrated to have some useful plasmonic properties in certain parts of the electromagnetic spectrum[20]), the simplest solution is to introduce a protective barrier layer between the metal and PCM layers, as we did for the GST-326 devices shown in Figure 6 (where we introduced an 8-nm Si_3N_4 layer between the PCM and the gold). To assess in more detail the role played by such barrier layers we deposited 40 nm thick Au films onto Si/SiO_2 substrates, then coated the Au films with thin (20 nm) GST-225 layers both with, and without, an intervening 8 nm Si_3N_4 barrier layer. Samples were then heated for 1 hour at 300°C, and thin cross-sections imaged in a transmission electron microscope (TEM). The results are shown in **Figure 9**, where it can be seen that complete assimilation of the Au and GST-225 layers occurred when no barrier was present, whereas the layers remained distinct in the presence of the barrier layer.

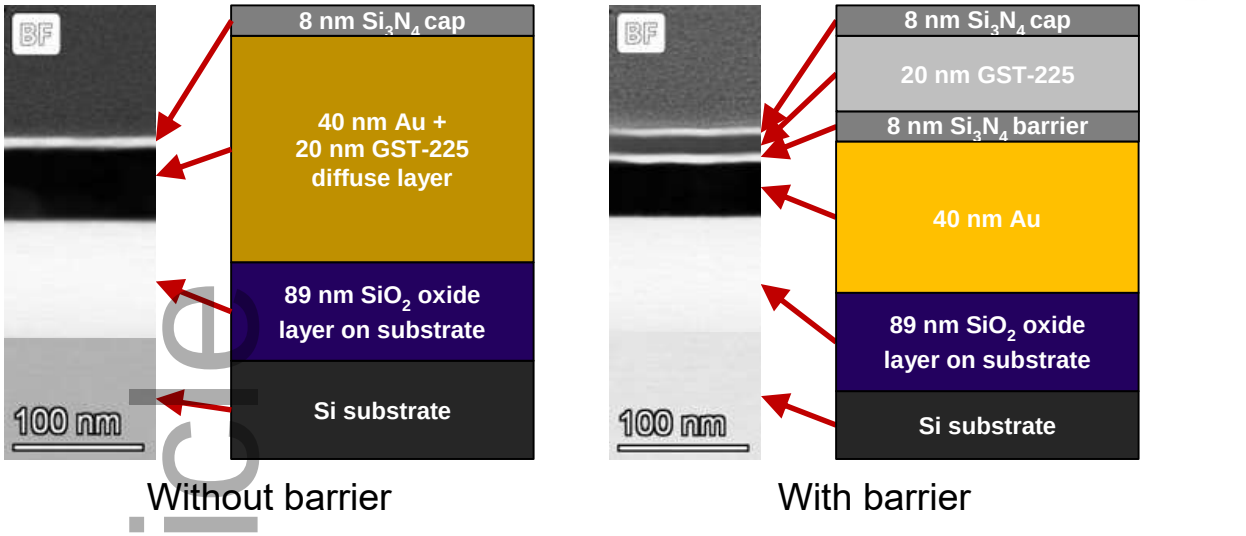

Figure 9. Cross-sectional TEM images, with corresponding schematics, of diffusion test samples (a) without and (b) with protective barrier layers

6. Conclusions

Actively-tunable EOT-PCM bandpass filters working in the mid-wave infrared were successfully designed, modelled, fabricated and tested. Such filters may find application in areas such as multispectral sensing and imaging, potentially providing much-reduced size and complexity as compared to conventional multispectral sensing approaches. A viable method for scaling-up of the fabrication of EOT arrays using a 'single-step' ultrafast laser ablation process was also demonstrated. Extending the concept of EOT-PCM based devices to the THz region showed that such devices might provide very useful modulation capabilities in this waveband. Finally, we re-iterated the importance of the proper provision of protective barrier layers in devices where gold and PCMs come into intimate contact. Without such barrier layers the heating that the PCM naturally undergoes when being switched between its states would almost certainly, in time, lead to interdiffusion and a consequent degradation of optical performance. We note that while in our devices (for demonstration purposes) switching was achieved by simple heating on a hotplate, in practical devices in-situ switching would undoubtedly be required/desired. Recently, various in-situ heating methods using embedded electrical micro-heaters have already been demonstrated for various PCM-based devices[21,22,23], and no-doubt such concepts can be extended to EOT-based devices, which have the inherent advantage of a (potentially current-carrying) metal layer being intrinsic to their structure. We also note that a thermally tunable EOT type effect has been reported in the microwave region by inserting dielectric meta-atoms (Mie resonators) in the centre of a subwavelength-sized aperture in a metallic waveguide[24], and it may be possible to adapt a such an approach to incorporate PCM materials.

Acknowledgements

Funding support is gratefully acknowledged from the EPSRC-QinetiQ TEAM-A Prosperity Partnership grant (EP/R004781/1), and from the EPSRC CDT in Metamaterials (EP/L015331/1). Thanks are also due to various University of Exeter colleagues, in particular Dr. Liam Trimby, Dr. Santiago Garcia-Cuevas Carrillo, Dr. Yat-Yin Au, Dr. Hong Chang, Dr. Prarthana Vadegadde Dakappa, Mr. Joe Shields, Mr. Joe Pady, Ms. Hannah Barnard and Prof. Geoff Nash, for contributing time, resources and expertise to various aspects of this work. We also thank Dr Geoff West of Warwick University, for providing cross-sectional TEM imaging.

[1] T. W. Ebbesen, L. Martín-Moreno, F. J. García-Vidal, H. J. Lezec, K. M. Pellerin, T. Thio, J. B. Pendry, *Nature* **1998**, 86, 6, pp. 1114-1117

[2] M. Rudé, V. Mkhitaryan, A. E. Cetin, T. A. Miller, A. Carrilero, S. Wall, F. J. G. de Abajo, H. Altug, V. Pruneri, *Advanced Optical Materials* **2016**, 4, 7, pp. 1060-1066

[3] L. Trimby, A. Baldycheva, C. D. Wright, *SPIE Proceedings* **2018**, 10541, February, pp. 105412B-1 - 105412B-8

[4] L. Deng, Z. Mao, X. Li, Z. Hu, F. Duan, Y. Yan, *ISPRS Journal of Photogrammetry and Remote Sensing* **2018**, 146, September, pp. 124-136

[5] S. Wong, J. Hopf, D. Kearney, *Proceedings of the 2004 Intelligent Sensors, Sensor Networks and Information Processing Conference* **2004**, pp. 195-198

[6] C. Gittins, W. Marinelli, *SPIE Proceedings* **1999**, January 1999, 3533, pp. 93-102

[7] H. Liang, *Applied Physics A: Materials Science and Processing* **2012**, 106, 2, pp. 309-323

[8] L. Lu, W. Dong, J. K. Behera, L. T. Chew, R. E. Simpson, *Journal of Materials Science* **2019**, 54, 8, pp. 2814-2823

[9] J. Shields, C. R. de Galarreta, J. Bertolotti, C. D. Wright, *Nanomaterials* **2021**, 11, 2, pp. 525-1-525-11

[10] H. A. Bethe, *Physical Review* **1944**, 66, 7-8, pp. 163-182

[11] F. Pryzbilla, A. Degiron, J-Y Laluet, C. Genet, T. W. Ebbesen, *J. Opt. A: Pure Appl. Opt.* **2006**, 8, 5, pp. 458-463

[12] S. G. Rodrigo, F. J. García-Vidal, L. Martín-Moreno, *Physical Review B* **2008**, 77, 7, pp. 075401-1 - 075401-8

[13] M. Tavakoli, Y. S. Jalili, S. M. Elahi, *Superlattices and Microstructures* **2019**, 130, pp. 454–471

[14] C. Ruiz de Galaretta, N. Casquero, E. Humphreys, J. Bertolotti, J. Solis, C. D. Wright, J. Siegel, *ACS Appl. Mater. Interfaces* **2022**, 14, 2, pp. 3446-3454

[15] A-K. U. Michel, M. Wuttig, T. Taubner, *Adv. Optical Mater.* **2017**, 5, pp.1700261-1 -1700261-8

[16] Y. Zhang, J. B. Chou, J. Li, H. Li, Q. Du, A. Yadav, S. Zhou, M. Y. Shalaginov, Z. Fang, H. Zhong, C. Roberts, P. Robinson, B. Bohlin, C. Ríos, H. Lin, M. Kang, T. Gu, J. Warner, V. Liberman, K. Richardson, J. Hu, *Nature Communications* **2019**, 10, 4276, pp. 1-9

[17] M. N. Julian, C. Williams, S. Borg, S. Bartram, H. J. Kim, *Optica* **2020**, 7, 7, pp. 746-754

[18] K. Makino, K. Kato, Y. Saito, P. Fons, A. V. Kolobov, J. Tominaga, T. Nakano, M. Nakajima, *J. Mater. Chem. C*. **2019**, *7*, pp. 8209-8215

[19] T. Cao, M. Lian, X. Chen, L. Mao, K. Liu, J. Jia, Y. Su, H, Ren. S, Zhang, Y. Xu, J. Chen, Z. Tian, D. Guo, *Opto-Electronic Science* **2022**, 1, 1, pp. 210010-1 – 210010-11

[20] S. Bagheri, C. M. Zgrabik, T. Gissibl, A. Tittl, F. Sterl, R. Walter, S. D. Zuani, A. Berrier, T. Stauden, G. Richter, E. L. Hu, H. Giessen, *Optical Materials Express* **2015**, 5, 11, pp. 7998-8006

[21] S. G-C. Carrillo, A. M. Alexeev, Y-Y. Au, C. David Wright, *Optics Express* **2018**, 26, 20, pp. 25567-2558

[22] Y. Zhang, C. Fowler, J. Liang, B. Azhar, M. Shalaginov, S. Deckoff-Jones, S. An, J. B. Chou, C. M. Roberts, V. Liberman, M. Kang, C. Ríos. K. A. Richardson, C. Rivero-Baleine, T. Gu, H. Zhang, J. Hu, *Nature Nanotechnology* **2021**, 16, 6, pp. 661-666

[23] N. Farmakidis, N. Youngblood, J. S. Lee, J. Feldmann, A. Lodi, X. Li, S. Aggarwal, W. Zhou, L. Bogani, W. H. P. Pernice, C. D. Wright, H. Bhaskaran *Advanced Science* **2022**, 9,20, pp. 2200383

[24] Y. Guo, H. Liang, X. Hou, X.Lv, L. Li, J. Li, K. Bi, M. Lei, J. Zhou, *Applied Physics Letters* **2016**, 108, 5, pp. 051906-1 - 051906-5

Humphreys et al., TOC text and image

Tunable mid- and long-wave infrared optical bandpass filters with potential applications in the area of multispectral sensing are designed and fabricated. The filters are based on the extraordinary optical transmission effect, with active tuning control provided by thermally switchable chalcogenide phase-change materials. Similar devices are also shown to act as useful modulators in the THz waveband.